Eur. Phys. J. E **21**, 231–242 (2006)
DOI 10.1140/epje/i2006-10063-7

THE EUROPEAN PHYSICAL JOURNAL E

Lateral vibration of a water drop and its motion on a vibrating surface

L. Dong[1], A. Chaudhury[2], and M.K. Chaudhury[1,a]

[1] Department of Chemical Engineering, Lehigh University, Bethlehem, PA 18015, USA
[2] Cornell University, Ithaca, NY, USA

Received 5 September 2006 and Received in final form 8 November 2006
Published online: 5 January 2007 –

Abstract. The resonant modes of sessile water drops on a hydrophobic substrate subjected to a small-amplitude lateral vibration are investigated using computational fluid dynamic (CFD) modeling. As the substrate is vibrated laterally, its momentum diffuses within the Stokes layer of the drop. Above the Stokes layer, the competition between the inertial and Laplace forces causes the formation of capillary waves on the surface of the drop. In the first part of this paper, the resonant states of water drops are illustrated by investigating the velocity profile and the hydrostatic force using a 3d simulation of the Navier-Stokes equation. The simulation also allows an estimation of the contact angle variation on both sides of the drop. In the second part of the paper, we investigate the effect of vibration on a water drop in contact with a vertical plate. Here, as the plate vibrates parallel to gravity, the contact line oscillates. Each oscillation is, however, rectified by hysteresis, thus inducing a ratcheting motion to the water droplet vertically downward. Maximum rectification occurs at the resonant states of the drop. A comparison between the frequency-dependent motion of these drops and the variation of contact angles on their both sides is made. The paper ends with a discussion on the movements of the drops on a horizontal hydrophobic surface subjected to an asymmetric vibration.

PACS. 47.55.D- Drops and bubbles – 47.61.-k Micro- and nano- scale flow phenomena – 68.08.Bc Wetting

1 Introduction

Recently, Daniel *et al.* [1,2] studied the movements of liquid droplets due to surface energy gradient in the presence of wetting hysteresis. Basic observation was that small liquid droplets do not move towards the more wettable part of the gradient, because they cannot overcome the force due to contact angle hysteresis. The hysteresis force on a gradient surface is, however, spatially asymmetric, its magnitude against the gradient being larger than that along the gradient. If a periodic force is applied to the drop, the force against the gradient is reduced whereas it is enhanced along the gradient; consequently the drops move with enhanced speeds towards the region of higher wettability. The situation is somewhat similar to the common observation that small water drops remain stuck on window panes or on plastic drinking cups even though they are attracted downward by gravity. The explanation of this effect in view of the early works by Frenkel [3] and others [4,5] lies, again, in wetting hysteresis. It is also a common observation that slight tapping of these surfaces often dislodges the water drops temporarily causing them to move downward, as the drops overcome the effect of hysteresis. The relationship between vibration and wetting hysteresis has been studied systematically by several investigators [6–9]. The general conclusion of these studies is that the wetting hysteresis can be partially or fully mitigated by vibration. This effect was used by Daniel *et al.* [1, 2] to induce motion of small drops on flat surfaces. Several other authors [10–12] have also demonstrated similar effects with an asymmetrically rough surface. In all these studies it has been found that matching of the forcing frequency with the natural frequency of drop vibration is critical to obtaining maximum rectification of the periodic disturbances by any asymmetric property of the surface, be it asymmetric roughness or wettability gradient.

The resonant frequencies of vibration of sessile or pendant liquid drops have in the past been studied extensively [13–23] due to their relevance to various technological processes, such as liquid–liquid extraction, synthesis of ceramic powders, crystal growth in microgravity, and the measurement of dynamic surface tension to name a few. The first basic result of oscillation of free liquid drops dates back to Kelvin [13] and Rayleigh [14]. Later Lamb [15], ignoring the viscous damping in the drop,

[a] e-mail: mkc4@lehigh.edu

developed a general expression for the different vibration modes of a free liquid drop as follows:

$$\omega = \sqrt{\frac{\gamma}{3\pi\, m} l(l-1)(l+2)}\,, \tag{1}$$

where ω is the resonant frequency, l is an integer value of 2 or higher, γ and m are the surface tension and mass of the drop, respectively. Later research by Strani and Sabetta [24] showed that a drop in partial contact with a surface has an extra low-frequency mode related to the center-of-mass oscillation. These authors [24] also showed that the solid support could also raise slightly the resonant frequencies of Rayleigh modes. Even though extensive efforts have been made to model the oscillation of drops in partial contact with a substrate undergoing vertical vibration, similar studies for the case of a drop undergoing lateral vibration are rather scanty. Nevertheless, a few recent studies [25–27] have made significant advances to this important problem. Lyubimov *et al.* [25] provided an elegant solution to the lateral oscillation of an inviscid drop by taking into account the oscillation of contact line. These authors predicted a low-frequency rocking vibration (rocking mode) of the drop in contact with a solid surface as well. Celestini and Kofman [26] analyzed this rocking mode quantitatively and compared their predictions with experimental observations. Moon *et al.* [27], on the other hand, identified a new mode associated with the rotational motion of the drop subjected to lateral oscillation.

Although not studied for lateral vibration, Noblin *et al.* [28] carried out a systematic study of the effect of vertical vibration of large water drops on a hydrophobic surface. These authors observed two types of behavior. At low amplitude, the contact line remains pinned and the drop presents various shapes, whereas at higher amplitude, the contact line exhibits an oscillatory motion by overcoming hysteresis. This type of oscillation, in the case of lateral vibration, leads to a net translation of the drop when the symmetry is broken either by hysteresis [1,2,10–12] or inertial forces [29].

In this paper, we investigate the resonant modes of a sessile water drop undergoing a lateral vibration using a 3d numerical simulation of Navier-Stokes equation. The velocity profile, hydrostatic force, and contact angle variation are investigated to identify the resonant states. We are particularly interested in finding out how much the contact angles of both sides of the drop differ and how they depend on the frequency of vibration, as it is this difference of the contact angles that determines the force and velocity of drops on surfaces. Finally, we attempt to make a qualitative comparison between the frequency-dependent contact angles of the vibrating water drop and its frequency-dependent motion induced by gravity. Finally we discuss a special case of drop motion induced by asymmetric vibration.

2 Mathematical formulation

We consider the oscillation of a sessile water drop vibrated parallel to the substrate as shown in Figure 1. When contact angle hysteresis is significant and the external force is sufficiently weak, the contact line remains pinned, but the water drop deforms. In order to elucidate the dynamics of the drop deformation, we used a FLUENT package to implement the numerical analysis, in which the 3d Navier-Stokes and continuity equations are solved using a well-established volume of fluid (VOF) model. Here we provide a brief description of the VOF model based on the detailed discussions of references [30] and [31]. In the VOF model, a single Navier-Stokes equation is solved along with the continuity equation for a domain comprising two fluid phases, which are water and air in our case. These equations are solved in conjunction with an extra VOF advection equation, in which a variable α, denoting the volume fraction of one of the phases is introduced. $\alpha = 1$ signifies that a given computational cell is filled with one of the phases (*i.e.* water), whereas $\alpha = 0$ signifies that the cell is filled with the other (air). The interface is tracked by the condition $0 < \alpha < 1$. The variables and properties of a computational cell are characterized by the volume-average values of the phases. The 3d Navier-Stokes, continuity, and VOF advection equations used to solve the problem of the oscillating drop are as follows:

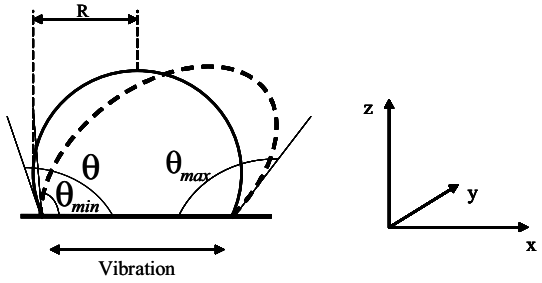

Fig. 1. Schematic of an oscillating drop on a vibrating substrate. The undisturbed profile of the drop is shown by the solid line, whereas the disturbed profile is shown by the dashed line. The contact line is assumed to remain pinned. The drop has an initial contact angle θ. θ_{max} and θ_{min} are, respectively, the maximum and minimum contact angles exhibited by the vibrating drop.

$$\frac{\partial}{\partial t}(\rho\mathbf{v}) + \nabla\cdot(\rho\mathbf{v}\mathbf{v}) = -\nabla p + \nabla\cdot[\eta(\nabla\mathbf{v}+\nabla\mathbf{v}^T)] - \rho g\mathbf{k}, \tag{2}$$

$$\frac{\partial\rho}{\partial t} + \nabla\cdot(\rho\mathbf{v}) = 0, \tag{3}$$

$$\frac{\partial\alpha}{\partial t} + \mathbf{v}\cdot\nabla\alpha = 0, \tag{4}$$

where $\mathbf{v} = (u, v, w)$ and p are velocity vector and pressure. $\rho = \rho^w\alpha + \rho^a(1-\alpha)$ is the density in the computational cell, ρ^w and ρ^a being the density of water and air, respectively. $\eta = \eta^w\alpha + \eta^a(1-\alpha)$ is the viscosity in the computational cell, η^w and η^a being the viscosity of water and air, respectively. $\mathbf{k} = (0, 0, 1)$ is a unit vector in the z-direction for horizontal vibration and $\mathbf{k} = (1, 0, 0)$ is a unit vector in the x-direction for vertical vibration. In order to account for the effect of the interface, a source term $\boldsymbol{f}$ is added to the right side of equation (2), which

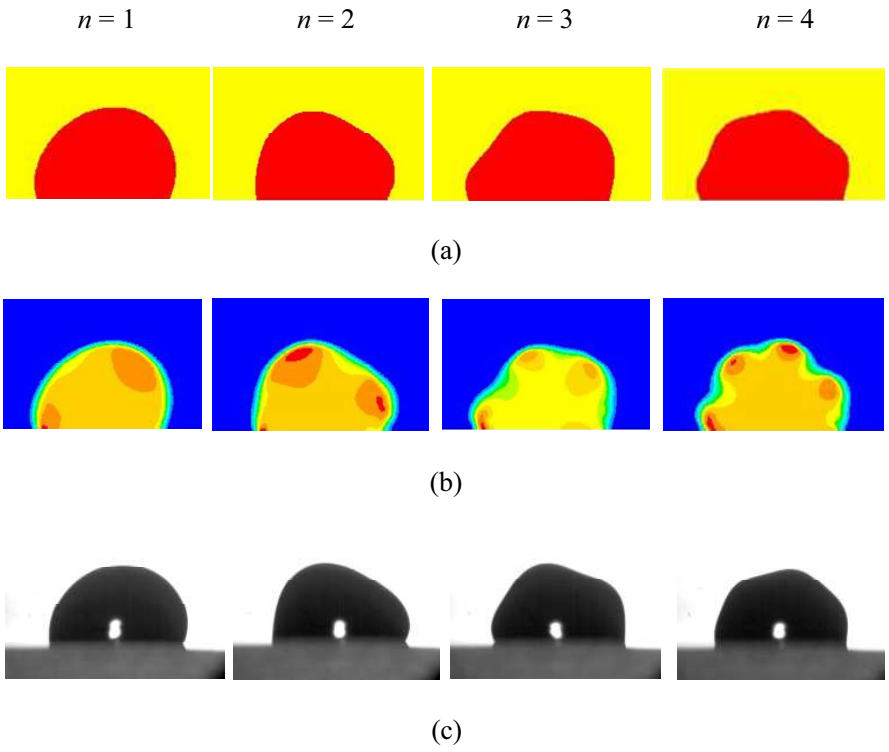

Fig. 2. First four resonance modes of a vibrating water drop: (a) simulated images, (b) pressure contours, and (c) experimental images. The first mode ($n = 1$) corresponds to the rocking mode. The second ($n = 2$), third ($n = 3$), and fourth modes ($n = 4$) here correspond to the Rayleigh first, second, and third modes, respectively. In (b), the pressure decreases from red color representing higher pressure to sky-blue representing lower pressure. The plate amplitude for these simulations is 0.5 mm, the diameter of the drop is 2 mm and the equilibrium contact angle is 110°. The images of the vibrating water drops as shown in panel (c) were captured using a high-speed camera (Midas) at a frame rate of 2000. The drops were placed on a horizontal silanized glass slide, which was vibrated along its long axis at an amplitude of 0.3 mm [32]. The details of the apparatus used for these studies have been described in references [2, 29] and [33].

is a volume force originating from the surface tension and curvature of the interface. This is the continuum surface force (CSF) model as developed by Brackbill *et al.* [31]. $\boldsymbol{f}$ is defined in the CSF model as

$$\boldsymbol{f} = \gamma \kappa \nabla \alpha \tag{5}$$

where γ is surface tension, and κ is the curvature of interface. According to equation (5), $\boldsymbol{f}$ is finite within a computational cell that contains the interface. Away from the interface it vanishes as $\nabla \alpha = 0$. In the CSF model, the interface curvature is calculated according to the outward unit normal vector $\mathbf{n}$ by

$$\kappa = -\nabla \cdot \mathbf{n}, \tag{6}$$

where $\mathbf{n} = -\nabla\alpha/|\nabla\alpha|$. The interface interpolation algorithm used in this study is the geometric reconstruction scheme, which tracks the interface using a piecewise linear approach as described in reference [30]. Using this scheme, the water-air interface is assumed to have a linear slope in each interface-containing computational cell. In the VOF model, the cells that contains the interface are first located by the condition $0 < \alpha < 1$. The position of the linear interface relative to the center of the cell is then calculated according to the volume fraction α and the unit normal vector $\mathbf{n}$.

The boundary conditions on the solid surface at $z = 0$ are the no-slip and the no-penetration conditions,

$$u = U_p\,, \qquad v = 0, \qquad w = 0 \tag{7}$$

where, U_p is the velocity of the vibrating substrate. For a sinusoidal periodic vibration, $U_p = 2\pi\omega A\cos(2\pi\omega t)$, A and ω being the amplitude of displacement and frequency of vibration, respectively. In the VOF model, the contact angle between the water and wall is defined by adjusting the curvature of the surface and the unit normal vector in the computational cells near a wall [30, 31].

In our study, the numerical analysis was carried out on a uniform rectangular mesh with the size of $40\,\mu$m $\times$ $40\,\mu$m$\times 40\,\mu$m, which was found to be optimum in terms of accuracy and computation time. We arrived at this mesh size after experimenting with various mesh sizes of decreasing order until the simulation result no longer depended on the mesh size. In the calculation, the pressure and velocity are coupled with pressure-implicit with splitting of operator (PISO) algorithm, which uses a guess-and-correct procedure for the calculation of pressure and a high degree of approximation relation between pressure

and velocity correction. A 2nd-order upwind scheme was used for the discretization of the model equations, which calculates the momentum quantity at the cell face from the value of the upstream cell using a second-order linear interpolation scheme [30].

3 Results and discussion

3.1 Drops on a vibrating horizontal surface

We first discuss the case where the water drop vibrates on a horizontal surface, *i.e.* the direction of vibration is perpendicular to that of gravity. After discussing various ways to identify the natural resonant frequencies of a liquid drop, we discuss in the next section the case of the drop on a vibrating vertical surface in which the drop moves down by gravity. In Section 3.3, we briefly discuss the drop motion on an asymmetric vibrating surface.

By varying the vibration frequency, the resonant modes of a water drop can be easily identified from the phase contour of the drop at different times. The shapes of a water drop at various resonant modes as obtained from the CFD simulation are compared with those obtained experimentally in Figure 2.

Here the first mode ($n = 1$) corresponds to the rocking vibration. The second ($n = 2$), third ($n = 3$), and fourth ($n = 4$) modes correspond to the Rayleigh first ($l = 2$), second ($l = 3$), and third ($l = 4$) modes, respectively. At the Rayleigh modes, regular capillary waves appear on the drop surface with its crests varying with the resonant modes. The pressure contours (Fig. 2b) also clearly highlight the different higher-pressure spots corresponding to various modes.

The understanding of the dynamics of a laterally oscillating drop can begin with the close observation of the profile of the horizontal velocity along the vertical direction (Fig. 3). The velocity profile for a 2 mm size drop corresponding to the vibration frequency of 130 Hz (Fig. 3) shows three characterized regions: the Stokes layer region ($\sim (2\mu/\rho\omega)^{1/2}$), the free-surface region, and a sublinear velocity gradient region. Within the Stokes layer, the fluid has a very large velocity gradient due to the diffusion of the substrate momentum. Above this layer, the fluid experiences an inertial force, which causes the drop to deform. The deformation is characterized by the oscillation of the center of mass, which leads to a contact angle difference between two sides of the drop (Fig. 1). The deformation is also associated with an increase of the surface area of the drop and the variation of the local curvature along the drop surface. Thus a restoring force arises due to the Laplace pressure acting inside the deformed drop, which attempts to decrease the surface area and restore the drop to its original shape. Competition of these two forces causes capillary waves to develop on the free surface. As Laplace pressure varies according to the local curvature, the velocity profile in the free-surface region shows an oscillating behavior. The drop performs something like a swinging oscillation of a one-end pivoted spring in the sublinear velocity gradient region. The drop deformation

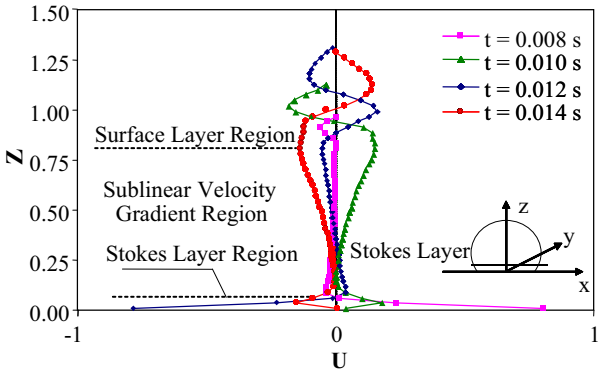

Fig. 3. Horizontal-velocity profile along the vertical direction in the central ($x = 0$ and $y = 0$) part of the drop at different times. These simulations were carried out with a drop of 2 mm diameter at a vibration frequency of 130 Hz. The plate amplitude and the equilibrium contact angle are 0.5 mm and 110°, respectively. The liquid-solid interface is at $z = 0$. Here, the dimensionless velocity, $U = u/U_p^*$, U_p^* being the maximum velocity of the plate ($2\pi A\omega$). The dimensionless vertical coordinate $Z = z/H$, where z is the dimensional vertical coordinate and H is the equilibrium height of the drop. The difference of the interface position is due to the evolving shape of the drop at different times. This plot shows that the momentum dissipation is confined within the Stokes layer ($\sim (2\mu/\rho\omega)^{1/2}$). The velocity profile of an oscillating drop can be roughly divided into three regions: Stokes layer, surface layer, and a sublinear velocity gradient region.

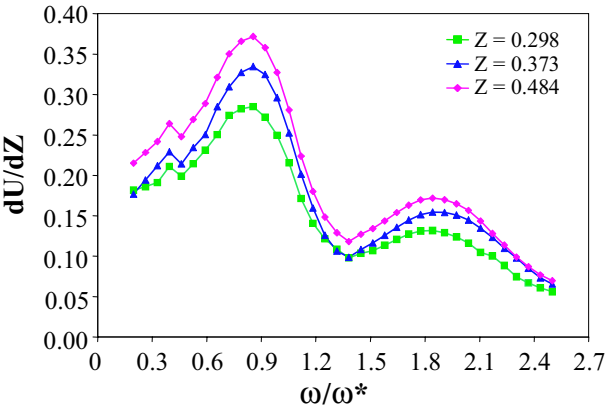

Fig. 4. The horizontal-velocity gradient along the vertical direction at different planes inside a vibrating drop *versus* the vibration frequency. U and Z are the dimensionless velocity and vertical distance, respectively. $\omega^* = (\gamma/m)^{1/2}$, where m is the mass of the drop. These are averages of maximum values of $\mathrm{d}U/\mathrm{d}Z$ obtained from several cycles, which are calculated at various values of Z as indicated in the figure. All these positions are outside the Stokes layer, and in the sublinear velocity gradient region. At resonant frequencies, the drop experiences larger deformation, thus larger velocity gradient [34]. The first three resonant frequencies are around 60 Hz, 130 Hz, and 290 Hz, respectively.

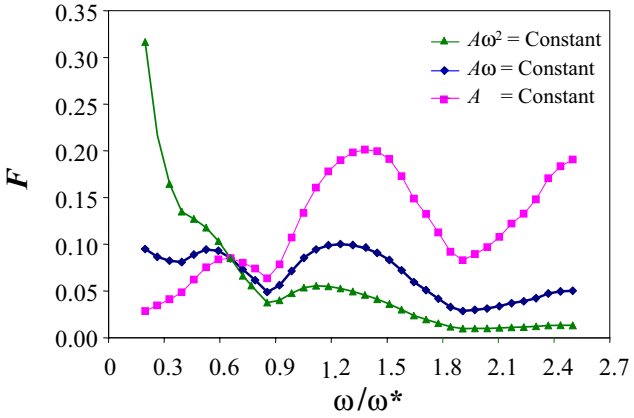

Fig. 5. The hydrostatic force (integration of pressure gradient over the entire drop) for a water drop of 2 mm diameter as a function of the vibration frequency. The dimensionless hydrostatic force $F = F^*/mg$, where F^* is the dimensional hydrostatic force, m is the mass of the drop as defined in Figure 4 and g is the gravitational acceleration. ω^* is defined in the caption of Figure 4. The figure shows that the hydrostatic force has minima at the resonant frequencies.

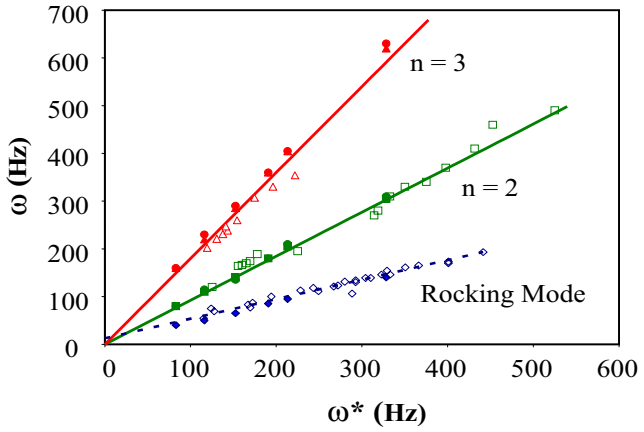

Fig. 6. The experimental and computed resonant frequencies of water drops as a function of ω^* or the mass of the drop. The open symbols correspond to the experimentally obtained data, which were reported previously by Daniel *et al.* [2,29,33]. The closed symbols correspond to the frequencies obtained from the CFD simulations for water drops of different masses (thus for different values of ω^*). The closed-diamond, closed-square, and closed-triangle symbols correspond to the frequencies obtained from the calculation of the hydrostatic force (as shown in Fig. 5). The closed-circle symbols correspond to the frequencies from the calculation of $\mathrm{d}U/\mathrm{d}Z$ (as shown in Fig. 4). Some of the simulated data calculated from two ways collapse together. The solid lines correspond to the first and second Rayleigh modes (Eq. (1)). The dashed line corresponds to the linear regression through the points corresponding to the experimental rocking-mode data.

can be characterized by the amplitude of this swinging oscillation, which can be quantitatively estimated from the velocity gradient. Moreover, one can compare the velocity gradients at different vibration frequencies to identify the resonant states. Figure 4 shows the vertical gradient of the horizontal velocity ($\mathrm{d}U/\mathrm{d}Z$) for a 2 mm diameter water drop as a function of the vibration frequency. As expected, the velocity gradient $\mathrm{d}U/\mathrm{d}Z$ exhibits a sinusoidal oscillation at the steady state. The $\mathrm{d}U/\mathrm{d}Z$ data reported in Figure 4 are the average maximum over several cycles at a specific frequency. All the three positions reported in Figure 4 are outside the Stokes layer, but are in the sub-linear velocity gradient region. It is evident from the data summarized in Figure 4 that the drop undergoes larger deformations at resonant frequencies compared to the non-resonant frequencies. Figure 4 identifies three resonant frequencies at 60 Hz, 130 Hz, and 290 Hz, respectively.

At any given instance, the inertial force of the entire drop is balanced by the pressure (hydrostatic) and viscous forces as shown in equation (8), which is the volume integral form of equation (2) (ignoring the gravitational term for horizontal vibration):

$$\rho\left(\int_V \mathbf{v}_t \mathrm{d}V + \int_V (\mathbf{v}\cdot\nabla)\,\mathbf{v}\mathrm{d}V\right) = -\int_V \nabla p \mathrm{d}V + \int_V \nabla\cdot\left[\eta\left(\nabla\mathbf{v} + \nabla\mathbf{v}^T\right)\right]\mathrm{d}V. \quad (8)$$

Numerical simulation shows that all the three terms of equation (8), *i.e.* the inertial force (the term on the left), the hydrostatic force (first term on right), and the viscous force (second term on the right), change at resonance, with the hydrostatic force varying with a different phase than the other two forces. While any of the above forces can be used to identify the resonance modes of a drop, we use the hydrostatic force to achieve this goal. Numerical simulations show that the hydrostatic force exhibits minima at resonance frequencies as shown in Figure 5. These minima are due to the fact that the pressure gradient in the Stokes layer is at 180° out of phase with that above the Stokes layer at resonance. Away from the resonance, this phase difference is less than 180°. This results in the maximum cancellation of the hydrostatic forces in the two regions at resonance, but not at non-resonance frequencies. In Figure 5, the hydrostatic force is non-dimensionalized by dividing it with the weight of the drop instead of $A\omega^2$, although non-dimensionalization with the latter would be a more logical thing to do. The objective here is to provide an idea of the magnitude of the hydrostatic force in comparison to the weight of the drop and to show that the position of the resonance frequency does not depend on the choice of either the constant amplitude A, constant $A\omega$, or constant $A\omega^2$ criterion. We, however, find that the plot with the constant $A\omega$ allows us to identify the peak position most clearly, which is therefore used in the subsequent analysis.

The resonance frequencies obtained from the maxima of the $\mathrm{d}U/\mathrm{d}Z$ values (Fig. 4), however, are in good agreement with those obtained from the minima of the hydrostatic force (Fig. 5). These data are summarized in Figure 6. As expected from equation (1), the resonant frequencies decrease with the drop mass following a square-root relationship, which conforms well to Lamb's

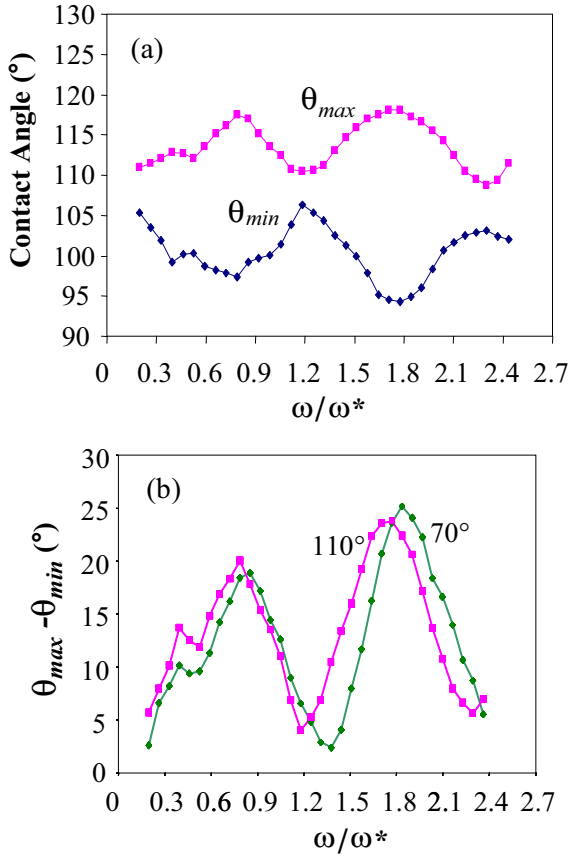

Fig. 7. Contact angle as a function of the vibration frequency for a water drop. (a) θ_{max} and θ_{min} correspond to the maximum and minimum angles at both sides of the drop when the equilibrium contact angle is 110°. (b) The contact angle difference $\theta_{max} - \theta_{min}$ for the equilibrium contact angle is 110° (solid squares) and 70° (solid diamonds). These calculations were carried out with drops of the same mass (3.2×10^{-6} kg). The solid lines are used only as a guide to the eye.

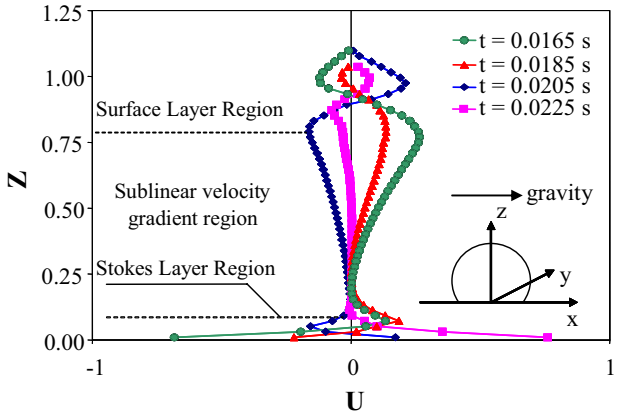

Fig. 8. Horizontal-velocity profile in the central ($x = 0$ and $y = 0$) part of a drop on a vertically vibrating surface. U and Z are defined in Figure 3. These calculations were carried out with a 2 μl size drop at a vibration frequency of 90 Hz. The plate amplitude and the equilibrium contact angle are 0.12 mm and 97°, respectively. This figure shows that the drop deforms more along the direction of gravity than against it. During the vibration, the plate experiences a maximum acceleration of 3.85 m/s^2, which is considerably lower than the magnitude of the gravitational acceleration (9.83 m/s^2).

analysis [15]. The CFD results also agree well with the experimental resonant frequencies of the drops as reported earlier by Daniel *et al.* [2,29,33]. Moreover, both the experimental and theoretical data show good agreement with the predictions based on Rayleigh equation (Eq. (1)) for the second and third modes (Rayleigh first and second modes).

Another method to identify the resonance frequencies was suggested by Celestini and Kofman [26], which is based on the examination of the contact angles on both sides of the vibrating drop. The difference of these angles exhibits maxima at the resonance frequencies, which were used by Celestini and Kofman [26] to identify the rocking mode of vibration of liquid mercury on glass. We used this approach to identify not only the rocking mode, but also the higher modes by following the frequency-dependent contact angles as obtained from the CFD simulated images of the oscillating drops. After capturing these images, the contact angles were measured using an image analysis program written in Matlab. As is the case with the velocity gradient, the contact angles on both the left and the right sides of the drop exhibit sinusoidal oscillation at steady state. θ_{max} (maximum contact angle) and θ_{min} (minimum contact angle) reported in Figure 7a are the average maximum and minimum values of both left- and right-side contact angles over several cycles. As anticipated (based on the analysis of Celestini and Kofman [26]), both θ_{max} and θ_{min} vary as a function of the vibration frequency. θ_{max} passes through maximum and θ_{min} passes through minimum values leading to large values for $\theta_{max} - \theta_{min}$ at the resonant frequencies. Thus, at the resonant frequencies, the two sides of an oscillating drop experience maximum contact angle differences. It is also important to notice that the general pattern of the behavior of the oscillating drop is not too sensitive to the equilibrium contact angle. For example, the resonant frequencies of a drop (3.2×10^{-6} kg) on a surface of equilibrium contact angle of 110° are about 4 to 8% lower than those obtained with a drop of the same mass, but with a lower equilibrium contact angle (70°) (Fig. 7b).

In the simulation, it was assumed that the drop remains pinned on the surface. In reality, when the contact angle difference between two sides of the drop is larger than the contact angle hysteresis, the drop would move relative to the vibrating substrate. Since the drop experiences larger contact angle difference at resonant frequencies, one expects that the drop would overcome the hysteretic threshold force most readily at the resonant frequencies and exhibit forward and backward motions relative to the vibrating substrate. With an asymmetric hysteresis or when an asymmetric inertial force acts on the drop, the drop should translate on the substrate with maximum velocities at the resonant frequencies.

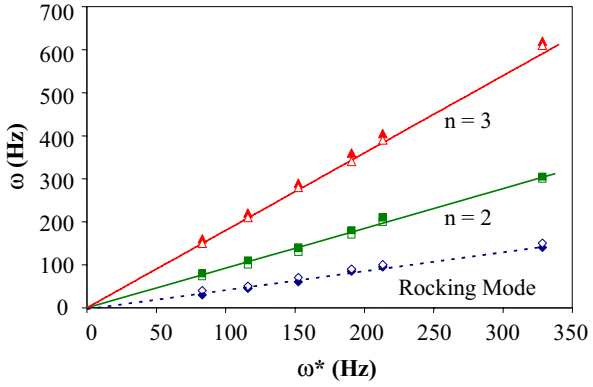

Fig. 9. The resonant frequencies of water drops on both the horizontal vibrating surface and the vertical vibrating surface as a function of ω^* or the mass of the drop. The closed symbols correspond to the horizontally vibrating surface, whereas the open symbols correspond to the vertically vibrating surface. The solid lines correspond to the first and second Rayleigh modes (Eq. (1)). The dashed line corresponds to the linear regression through the points corresponding to the data of the rocking mode for the drop on a horizontal vibrating surface. ω^* is defined in Figure 4.

3.2 Drops on a vibrating vertical surface

The CFD simulation of a drop on a vibrating vertical plate (Fig. 8 inset) was carried out as before, except that the gravity now acts parallel to vibration. During the first half of the stroke, the inertial and the gravitational forces jointly deform the drop, whereas during the next half of the stroke, the inertial force is reduced by gravity. Overall, the drop vibrates asymmetrically as is shown by the non-symmetrical velocity distribution inside the drop during the forward and reverse cycles (Fig. 8).

The resonance frequencies of the drop oscillating vertically were determined as before from the integration of the pressure gradient. The results summarized in Figure 9 show that these resonance frequencies are not noticeably different from those of the horizontal vibrations. A similar picture emerges from the contact angles of the drop as well. Figure 10a plots the largest difference of the contact angles for a 2 μl drop on both sides of the drop as a function of frequency. As expected, a larger difference of the contact angles occurs when the drop trajectory is downward as opposed to the upward movement. Although the frequencies corresponding to the first, second and third modes are not all that different from that of the horizontal vibration, the amplitude of the drop vibration corresponding to each resonance is higher for the case of vertical vibration. Furthermore, the first mode (*i.e.* the rocking mode) for the case of asymmetric vibration is considerably stronger than the second mode, which is opposite to the trend observed with the vibration on the horizontal surface.

Apparently, some of the gravitational energy is channeled to the vibration modes of the drop during this asymmetric vibration. Furthermore, the strengthening of the first peak relative to the second is indicative of the energy exchange between the two modes. These simulation results, however, could not be confirmed in the same way as that of the horizontal vibration since the large drops move down by gravitational force and the small drops move downward in the presence of vibration. The simulation results, however, have important implications with respect to the vibration-induced motion of drops on vertical surfaces [35], which provide an indirect test of the simulation results. In order to understand the implications of these results, we have conducted a simple experiment with a small liquid droplet on a homogeneous surface inclined vertically. The surface is a silanized silicon wafer, which exhibits advancing and receding contact angles with water

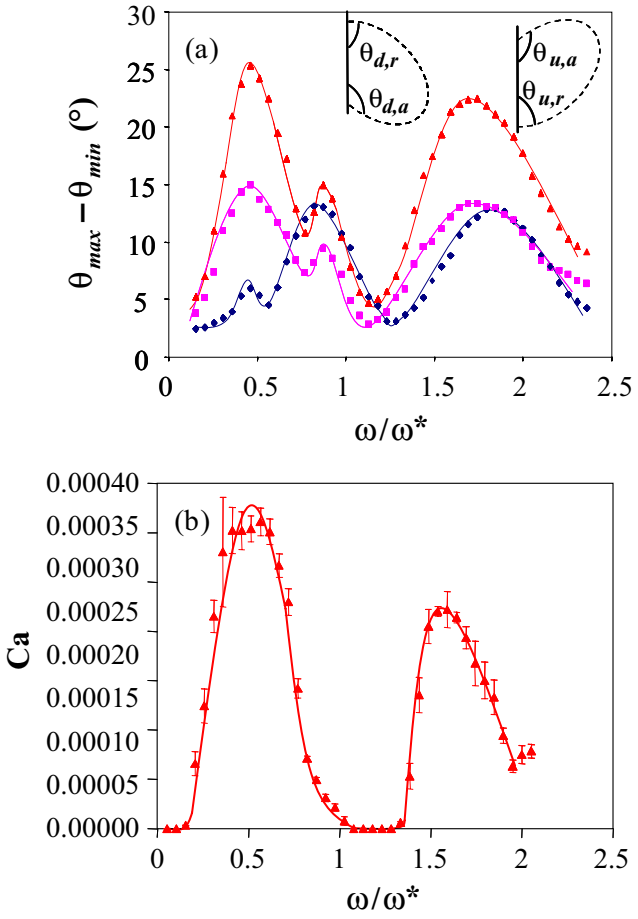

Fig. 10. (a) Simulated contact angle difference as a function of the vibration frequency for a 2 μl water drop subjected to a vibration on a horizontal (solid diamond) and vertical surface. Here, the solid triangle and solid square correspond to the downward and upward movements of the drop, respectively. (b) The experimental velocities of a 2 μl drop moving vertically downward on a vibrated surface. The surface was a silanized silicon wafer. In all cases, the maximum vibration velocity ($2\pi A\omega$) is 69 mm/s, while the maximum plate acceleration changes from 1.3 m/s^2 at 30 Hz to 13.0 m/s^2 at 300 Hz. The average of the advancing and receding contact angles at rest is 97°. All the simulations of panel (a) were performed with the equilibrium contact angle of 97°. The solid lines are used only as a guide to the eye.

of 104° and 89° (15° hysteresis), respectively. Small drops of water ($\sim 2\,\mu$l) remain stuck to this surface because the hysteresis force wins over the gravity force. However, as the plate is vibrated, the contact line oscillates asymmetrically. Each oscillation is rectified [36] by hysteresis and the drop moves downward with a speed depending on the frequency of vibration. When the drop speed is plotted as a function of frequency, clear velocity maxima could be identified at the resonance modes of vibration. Figure 10b summarizes these results, where the velocity (V) of the drop is non-dimensionalized by dividing it with the capillary velocity (γ/η) to yield the capillary number $Ca(V\eta/\gamma)$. It should be noted that the actual velocity of a drop varies with time. V represents the average drift velocity.

In agreement with simulation results, the most intense velocity peaks correspond to the first and third resonances, respectively. As a first-order approximation, the velocity of the drop (or Ca) is proportional to the difference of the cosines of dynamic receding and advancing angles [37,38]. However, as discussed in reference [29], some amount of wetting hysteresis is necessary to break the symmetry of any periodic pulse. Thus, for the discussion to follow, we assume that a small hysteresis is intrinsically present at the contact line. The discussion to follow is not correct in its detailed features, but it provides an approximate framework with which to examine the droplet motion. We consider that the ultimate effect of all the hydrostatic, inertial and viscous forces is to modify the local contact angles on the two sides of the drop. Let θ be the intrinsic Young's contact angle, and $\theta_{d,r}$ and $\theta_{d,a}$ be the receding and advancing contact angles of the drop during the first half of the downward stroke of the drop. If $\theta_{d,a} > \theta$ and $\theta_{d,r} < \theta$, uncompensated forces would act on the advancing and receding edges, the magnitudes of which are $\gamma(\cos\theta - \cos\theta_{d,a})$ and $\gamma(\cos\theta_{d,r} - \cos\theta)$, respectively, per unit length. The net uncompensated force experienced by the drop is $\sim \gamma R(\cos\theta_{d,r} - \cos\theta_{d,a})$, R being the base radius of the drop. If most of the resistance to the motion of the drop arises from the contact line region, the viscous drag force experienced by the drop is proportional to ηRV. Balance of the above two forces leads to $Ca_d \sim \cos\theta_{d,r} - \cos\theta_{d,a}$, where Ca_d is the capillary number corresponding to the downward motion of the drop. During the other half of the stroke, $Ca_u \sim \cos\theta_{u,r} - \cos\theta_{u,a}$ (here the subscript u denotes upward). Note that in the above expressions, both $\theta_{d,r}$ and $\theta_{u,r}$ have to be smaller than the intrinsic receding angle (θ_r), and both $\theta_{d,a}$ and $\theta_{u,a}$ have to be larger than the intrinsic advancing angle (θ_a) before the drop moves on the surface. The net velocity is obtained from the difference of the above two terms, *i.e.* $Ca \sim (\cos\theta_{d,r} - \cos\theta_{d,a}) - (\cos\theta_{u,r} - \cos\theta_{u,a})$.

In Figure 11, the experimentally obtained capillary numbers are compared with the driving force $[(\cos\theta_{d,r} - \cos\theta_{d,a}) - (\cos\theta_{u,r} - \cos\theta_{u,a})]$. Again, the general trends of both sets of data are very similar and the positions of the experimentally obtained velocity peaks corresponding to the first and third resonance show a very good correlation with those of the driving forces. There is, however, a discrepancy. The computational analysis predicts a small velocity peak corresponding to the second resonance, which is absent in the experimental velocity spectrum. There could be various sources for this discrepancy. First of all, our experiments may not have the required sensitivity to detect small differences of velocity to properly identify the second peak. Secondly, the computational analysis has been carried out with pinned contact line and by ignoring wetting hysteresis. Hysteresis, which is the key to obtaining rectification [29] of periodic pulses, also suppresses or obliterates any excitation less than the threshold force.

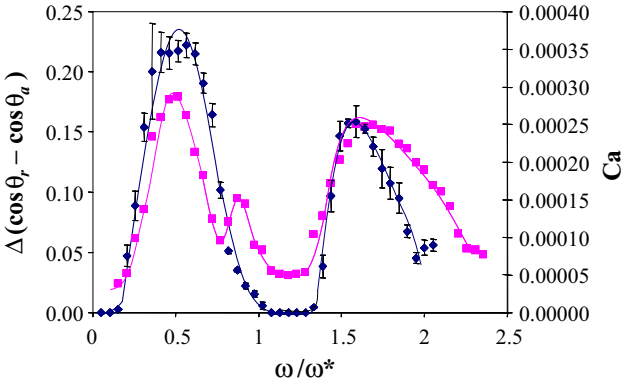

Fig. 11. The experimental velocities (solid diamond) of a $2\,\mu$l water drop moving on a vibrating vertical surface are compared with the characteristic driving force (solid square) as a function of vibration frequency. Here, $\Delta(\cos\theta_r - \cos\theta_a) = (\cos\theta_{d,r} - \cos\theta_{d,a}) - (\cos\theta_{u,r} - \cos\theta_{u,a})$ (see Fig. 10a for the definitions of subscripts.) The velocity as well as the forcing frequency are non-dimensionalized as Ca and ω/ω^*, Ca is defined in the text and ω^* is defined in Figure 4. The solid lines are used only as a guide to the eye.

For reasons related to hysteresis, there are some differences between the numerically obtained contact angles and those found experimentally. Figure 12 summarizes the variations of the experimentally obtained contact angles of the two sides of the drop for oscillation frequencies of 110 Hz, 230 Hz, and 310 Hz, respectively. The velocity of the drop is maximum at 110 Hz ($\omega/\omega^* = 0.56$) which corresponds to the first resonance mode. According to the numerical simulation, the maximum difference of the contact angles, at this frequency, should fluctuate between $+25°$ and $-15°$, respectively. The experimental values, on the other hand, fluctuate between $+44°$ and $-26°$, respectively. In the presence of hysteresis, the drop undergoes a larger deformation as one of the edges approaches the advancing angle, which is larger than the equilibrium angle, whereas the other edge approaches the receding angle, which is smaller than the equilibrium angle. The driving forces along both the downward and upward directions are, however, reduced and the corresponding capillary numbers are described by: $Ca_d \sim (\cos\theta_{d,r} - \cos\theta_{d,a}) - H$, and $Ca_u \sim (\cos\theta_{u,r} - \cos\theta_{u,a}) - H$, respectively. Here H signifies a hysteresis threshold that needs to be overcome for the drop to move. The net capillary number is,

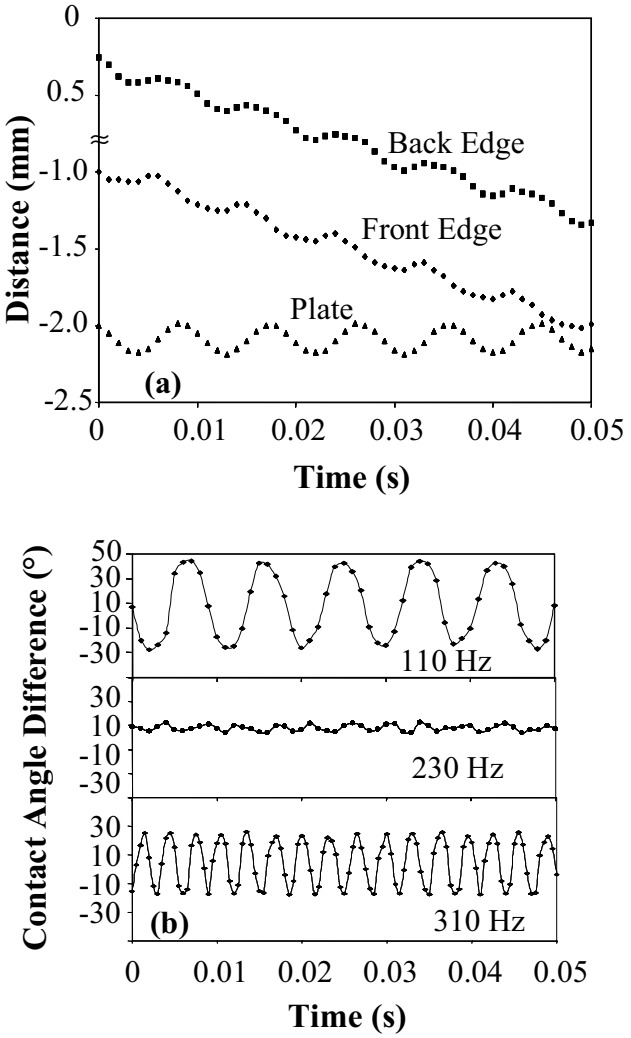

Fig. 12. (a) Periodic rectification of the advancing and receding edges of a 2 μl water drop on a vertical surface subjected to a vibration frequency of 110 Hz. The tracking of both edges of the drop was performed with a high-speed camera at a frame rate of 2000. The positions of both the advancing and receding edges were performed relative to a fixed reference point. In each cycle of vibration, both the advancing and receding contact line oscillates on the surface, but with a net drift downwards. The differences of the contact angles between the bottom and upper edges of the drop were estimated from the video frames captured with a high-speed camera (2000 fps). Typical results obtained for the vibration frequencies of 110 Hz, 230 Hz, and 310 Hz are shown in panel (b).

however, given by the following equation:

$$Ca \sim \frac{1}{\tau} \oint [(\cos\theta_r - \cos\theta_a) - H] \mathrm{d}t, \qquad (9)$$

where τ is the period of oscillation. In equation (9), only positive values of $(\cos\theta_r - \cos\theta_a) - H$ are considered, as the drop cannot move during the duration for which $(\cos\theta_r - \cos\theta_a) < H$. We thus have stop-go events: the drop moves when $(\cos\theta_r - \cos\theta_a) > H$, but it stops when $(\cos\theta_r - \cos\theta_a) < H$. This jump discontinuity is important in order to achieve a net drift motion of the drop as has been discussed in reference [29]. It is possible that during half of a cycle $(\cos\theta_r - \cos\theta_a) > H$, in which case the drop would move downward. However, during the other half of the cycle $\cos\theta_r - \cos\theta_a < H$, in which case there is no driving force on the drop, thus it remains stuck on the surface. The evaluation of the cyclic integration needs to reflect the above facts. However, if the drop moves relative to the substrate in both the downward and upward directions, as is the case at the first and third resonance frequencies, its net drift velocity (expressed in terms of Ca) is approximately given by the difference of Ca_d and Ca_u. In this case, the hysteresis term H nearly cancels out and one obtains the same expression as that on the non-hysteretic surface as discussed in references [2] and [3]. Based on the advancing and receding contact angles ($\theta_{d,r} = 68°$, $\theta_{d,a} = 113°$; $\theta_{u,r} = 73°$, $\theta_{u,a} = 100°$) on the right and left sides of the drop, the term $[(\cos\theta_{d,r} - \cos\theta_{d,a}) - (\cos\theta_{u,r} - \cos\theta_{u,a})]$ is estimated to be about 0.3 at the first resonance peak. This leads to an estimate of the constant of proportionality between the capillary number ($Ca \sim 0.00035$) and $[(\cos\theta_{d,r} - \cos\theta_{d,a}) - (\cos\theta_{u,r} - \cos\theta_{u,a})]$ as 0.0012. Using a similar approach, the above proportionality factor at the third resonance is about 0.002. These proportionality constants are indicative of the frictional resistance experienced by the drop, a part of which originates at the contact line. Recently, Daniel *et al.* [2] studied the motion of liquid drops of various viscosities driven by a gradient of the surface energy. From these studies, the constant of proportionality between the capillary number and the driving force $(\cos\theta_a - \cos\theta_r)$ can be estimated to be about 0.005. Using a correction factor that comes from the fact that an oscillating drop on the average experiences a driving force that is π times [39] lower than $[(\cos\theta_{d,r} - \cos\theta_{d,a}) - (\cos\theta_{u,r} - \cos\theta_{u,a})]$, we expect a proportionality factor between capillary number and driving force to be 0.0016, which roughly corresponds to the numbers reported above. This should, nevertheless, be considered as a crude analysis at present as we have not considered the energy dissipation occurring within the thin Stokes layer adjacent to the substrate.

Overall, the intense velocity peak at the first resonance, as predicted by the numerical simulation, is consistent with the experimental observation. However, as mentioned above, there are some disagreements between the simulations and experiments, which are due to various reasons. Most significantly, the base of the drop is pinned in our simulation. With the simulated results obtained with pinned drops, we assumed that the drop would move as long as the maximum difference of the contact angles on both sides of the drop is larger than hysteresis. Secondly, the role of contact angle hysteresis has not been explicitly taken into account in our simulation. As mentioned above, hysteresis should allow a much larger deformation of the drop as one of its edge tries to attain the advancing angle while the other edge tries to achieve the receding angle, all of which resulting in a larger asymmetric vibration. This larger asymmetry could excite the first resonance (*i.e.* the rocking mode) even more strongly, and

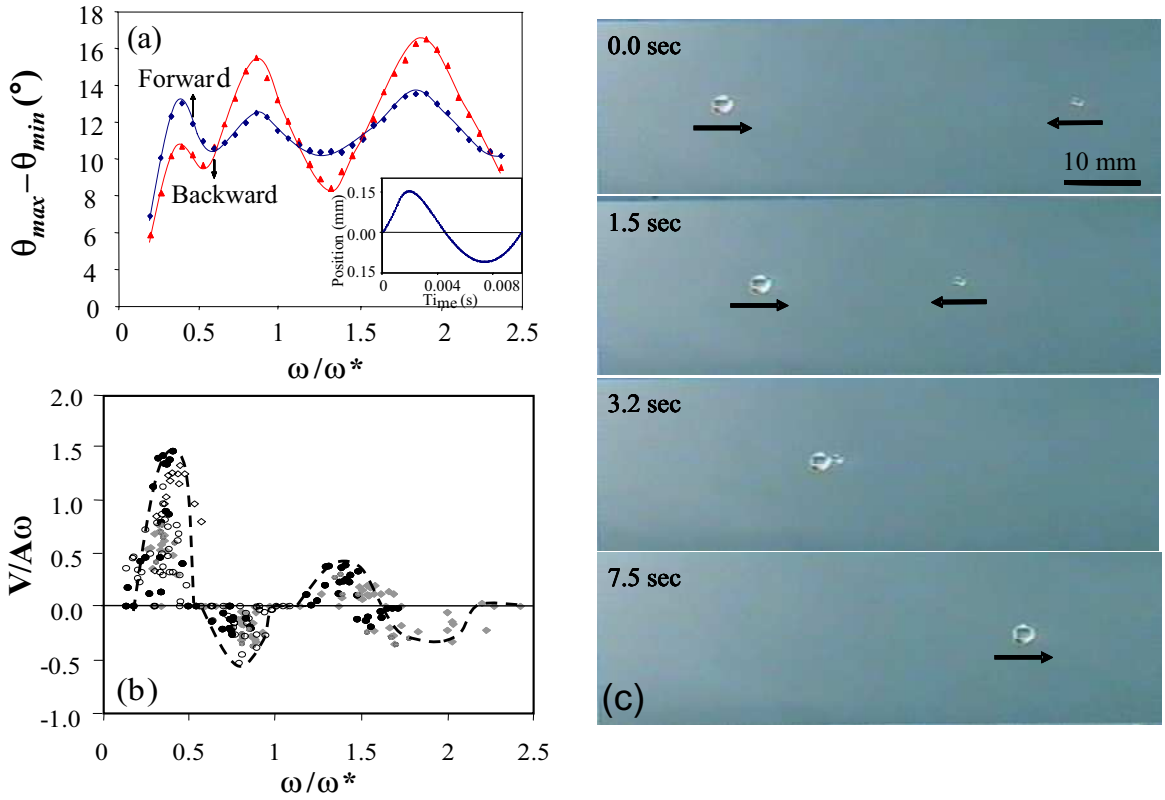

Fig. 13. (a) The difference between the contact angles of the right and the left sides of a drop subjected to an asymmetric vibration (see inset). These simulations were carried out with a small drop of 2 mm diameter. The equilibrium contact angle is 110°. Here, three resonant frequencies are observed at 60 Hz, 130 Hz, and 290 Hz, respectively. Based on these contact angles, it is expected that the drop would move forward when ω/ω^* is about 0.40, but move backward when it is about 0.85. Another reversal of drop motion is expected to occur at ω/ω^* and 1.90. Panel (b) (adapted from Ref. [29] with a slight modification) provides the experimental data of drop motion that is in qualitative agreement with the prediction of panel (a). Panel (c) shows that two dissimilar-size drops indeed move in the opposite directions when excited by an asymmetric waveform (100 Hz) of the type shown in panel (a). ω/ω^* of the smaller drop (~ 0.68) corresponds to its second resonance mode, whereas that (~ 1.35) of the larger drop corresponds to the pre-resonance of the third mode.

suppress the second mode, as is found experimentally. Estimation of the intrinsic hysteresis is, however, a major limitation of the problem, as the release of the contact line from metastable energy barriers that gives rise to hysteresis may depend on vibration frequency as well.

3.3 Drop motion using asymmetric vibration: polarized ratchet

The enhancement of the first resonance compared to the second in the presence of an external force, such as gravity, could lead to several interesting possibilities. If, for example, a Maxwell stress or an inertial stress is set up in the drop and if this stress is switched on and off with a time-varying asymmetry, it may be possible to induce a strong first resonance in one instance, but a stronger second resonance in another instance. Thus, depending upon the strengths of these external excitations, the drop may be induced to go forward or backward. A situation somewhat like that speculated above was recently observed by Daniel *et al.* [29,33]. These authors examined the fate of a drop vibrated on a hydrophobic surface with an asymmetric waveform. The particular waveform used by these authors is either a sawtooth or an exponential fall/rise wave that accelerates the plate fast in one stroke, but decelerates it slowly in the other. The resulting asymmetric inertial force was rectified by hysteresis thus inducing a motion of the drop on the surface. Daniel *et al.* [29,33] observed that the direction of the motion of the drop depends on the frequency of vibration and the size of the drop. One of the most interesting observations was that two drops of dissimilar sizes travel in the opposite directions at a given frequency. This is what we denote here as a polarized ratchet. A plausible explanation of this effect could be due to the asymmetric amplification of modes, as is the case with a drop moving down by gravity. In order to test this hypothesis, we carried out a numerical solution of a drop on a surface undergoing asymmetric vibration (fast linear rise and exponential fall of acceleration) using the methodologies described in the above sections. The motion of the vibrating plate resulting from such a waveform is shown in the inset of Figure 13a, which was input in the simulation as a Fourier series. The contact angles of

a small drop (2 mm diameter) exhibited three resonance modes at 60, 130 and 290 Hz, respectively, which are the same as those of symmetric periodic vibrations (Fig. 4). Interestingly, however, the intensities of these modes during the forward and the backward strokes exhibit an oscillatory behavior. For example, while the first rocking mode is stronger during the forward stroke, the second mode is stronger in the reverse stroke. Another reversal of order occurs near the third resonance. The consequence of all of these is that a drop of a given size should move in one direction at its first resonance frequency, but in the opposite direction at the second resonance. If the frequency is kept constant, two different-size drops, the resonance frequencies of which correspond to first and second modes, respectively, move in opposite directions as shown in Figure 13c.

4 Conclusions

Numerical analysis of the 3d Navier-Stokes equation has been useful in identifying the resonance modes of vibration of a sessile drop on a hydrophobic surface. The vibration mode can be identified in various ways, *i.e.* calculating the velocity gradient, the net hydrostatic force across the drop or just by finding the extreme values of the contact angles on both sides of the drop. The resonant frequencies identified from these simulations are in good agreement with the experimental results reported previously [2,29,33].

A remarkable finding of the simulations with a drop on a vibrating vertical surface is that gravity enhances the first resonant mode and weakens the second mode, even though the positions of the resonance peaks do not differ substantially from those observed with the horizontal vibrations. These results are in qualitative agreement with the experimental observations of drops moving downward on a vibrating surface. When a drop is vibrated on a horizontal surface with an asymmetric vibration, different modes are asymmetrically amplified during the forward and reverse strokes of a vibration cycle. These asymmetries lead to what we term as "polarized ratchet", in which drops of different sizes move in opposite directions.

The current analysis is however limited by the fact that the contact line is pinned. In reality, the contact line would slip on the surface whenever the dynamic angle is larger than the advancing, or lower than the receding angle. A detailed analysis of the problem by taking care of the contact line slippage and contact angle hysteresis is a natural extension of this study; however, all these parameters are non-linearly coupled to each other. If successfully carried out, such an analysis would shed considerable light on the vibrated motion [29] of liquid drops on surfaces due to asymmetric hysteresis or inertial force on quantitative terms.

L.D. was supported by a grant from PITA (Pennsylvania Infrastructure Technology Alliance). M.K.C. acknowledges many discussions with F. Celestini and thanks him for sharing his work with us prior to publication. Some of the ideas regarding the role of hysteresis in drop motion resulted from some earlier suggestions by Prof. P.G. de Gennes (see Ref. [29]). All the numerical simulations of this work were carried out by L.D. The experiments with the motion of a drop on a vertical surface and the related analysis were carried out by A.C.

References

1. S. Daniel, M.K. Chaudhury, Langmuir **18**, 3404 (2002).
2. S. Daniel, S. Sircar, J. Gliem, M.K. Chaudhury, Langmuir **20**, 4085 (2004).
3. Y.I. Frenkel, J. Exp. Theor. Phys. (USSR) **18**, 659 (1948), translated into English by V. Berejnov (`http://arxiv.org/ftp/physics/papers/0503/0503051.pdf`).
4. J.J. Bikerman, J. Colloid Sci. **5**, 349 (1950).
5. C.G.L. Furmidge, J. Colloid Sci. **17**, 309 (1962).
6. T. Smith, G. Lindberg, J. Colloid Interface Sci. **66**, 363 (1978).
7. C. Andrieu, C. Sykes, F. Brochard, Langmuir **10**, 2077 (1994).
8. E.L. Decker, S. Garoff, Langmuir **12**, 2100 (1996).
9. T.S. Meiron, A. Marmur, I.S. Saguy, J. Colloid Interface Sci. **274**, 637 (2004).
10. O. Sandre, L. Gorre-Talini, A. Ajdari, J. Prost, P. Silberzan, Phys. Rev. E **60**, 2964 (1999).
11. A. Buguin, L. Talini, P. Silberzan, Appl. Phys. A: Mater. Sci. Processing **75**, 207 (2002).
12. A. Shastry, M.J. Case, K.F. Böhringer, Langmuir **22**, 6161 (2006).
13. Lord Kelvin, Math. Phys. Pap. **3**, 384 (1890).
14. Lord Rayleigh, *The Theory of Sound* (Macmillan, 1894).
15. H. Lamb, *Hydrodynamics* (Cambridge University Press, UK, 1932).
16. S. Chandrasekhar, *Hydrodynamic and Hydromagnetic Stability* (Dover, Mineola, NY, 1961).
17. V.I. Kalechits, I.E. Nakhutin, P.P. Poluektov, Sov. Phys. Tech. Phys. **29**, 934 (1985).
18. R.W. Smithwick, J.A.M. Boulet, J. Colloid Interface Sci. **130**, 588 (1989).
19. V.I. Kalechits, I.E. Nakhutin, P.P. Poluektov, Yu.G. Rubezhnyi, V.A. Chistyakov, Sov. Phys. Tech. Phys. **5**, 496 (1979).
20. N. Yoshiyasu, K. Matsuda, R. Takaki, J. Phys. Soc. Jpn. **65**, 7 (1996).
21. O.A. Basaran, D.W. DePaoli, Phys. Fluids **6**, 2923 (1994).
22. E.D. Wilkes, O.A. Basaran, Phys. Fluids **9**, 1512 (1997).
23. H. Rodot, C. Bisch, A. Lasek, Acta Astronautica **6**, 1083 (1979).
24. M. Strani, M.F. Sabetta, J. Fluid Mech. **141**, 233 (1984).
25. D.V. Lyubimov, T.P. Lyubimova, S.V. Shklyaev, Fluid Dyn. **39**, 851 (2004).
26. F. Celestini, R. Kofman, Phys. Rev. E **73**, 041602 (2006).
27. J.H. Moon, B.H. Kang, H.Y. Kim, Phys. Fluids **18**, 021702 (2006).
28. X. Noblin, A. Buguin, F. Brochard-Wyart, Eur. Phys. J. E **14**, 395 (2004).
29. S. Daniel, M.K. Chaudhury, P.G. De Gennes, Langmuir **21**, 4240 (2005).
30. Fluent 6.2 User's Guide, Fluent Inc., 2003.
31. J.U. Brackbill, D.B. Kothe, C. Zemach, J. Comput. Phys. **100**, 335 (1992).

32. The images were taken at 0.3 mm plate amplitude rather than at higher amplitudes because of two reasons. Firstly, we tried to avoid the distortion of the forcing signals that sometimes develop at higher amplitudes in our experimental apparatus. Secondly, wetting hysteresis allows a larger deformation of the drop than the simulations. When we impose the condition of pinned contact line, we mean that the contact angle at the three phase contact line is pinned to a certain value. All the macroscopically observable changes are due to the dynamic deformation of the drop. In reality, however, the contact angle on each edge of the drop is bound by two extreme values with multiple metastable angles in between. We expect a larger deformation of the drop in a real system because the metastable angles on each side can switch between two extremes values. Nevertheless, the resonant vibration frequencies and the overall pattern exhibited by the vibrating drop are not affected by the amplitude of vibration in both simulations and experiments.
33. S. Daniel, *The Effect of Vibration on Liquid Drop Motion*, PhD Thesis, Lehigh University, 2005.
34. We checked the linear response of the drop vibration in various ways. Particularly, we calculated the velocity gradient at a given frequency and the fixed position inside the drop and observed a linear correlation between the velocity gradient and vibration amplitude.
35. Vibration-induced motion of objects in a gravitational field for solid-solid case, where symmetry is broken by solid friction has recently been studied by Buguin *et al.*: A. Buguin, F. Brochard, P.G. De Gennes, Eur. Phys. J. E **19**, 31 (2006).
36. Some elegant studies of the contact line oscillation in another system involving Faraday waves in a glass container were reported previously. See C.-L. Ting, M. Perlin, J. Fluid Mech. **295**, 263 (1995); L. Jiang, M. Perlin, W.W. Schultz, Phys. Fluids **16**, 748 (2004). In the paper by Jiang *et al.*, the authors report a non-linear relationship between wave frequency and amplitude near contact lines. We suspect that a similar non-linearity may also be present in our studies. However, we have not investigated this effect systematically this time.
37. H.P. Greenspan, J. Fluid Mech. **84**, 125 (1978).
38. F. Brochard, Langmuir **5**, 432 (1989).
39. In either the downward or upward direction, the average force is $\frac{2}{\pi}$ times the maximum force. However, this force is divided by 2 as the drop moves forward half of the cycle and backward for the other half.